

MIT Open Access Articles

*Theoretical and experimental investigation
of haze in transparent aerogels*

The MIT Faculty has made this article openly available. **Please share**
how this access benefits you. Your story matters.

As Published: 10.1364/OE.27.000A39

Publisher: The Optical Society

Persistent URL: <https://hdl.handle.net/1721.1/135137>

Version: Final published version: final published article, as it appeared in a journal, conference proceedings, or other formally published context

Terms of Use: Article is made available in accordance with the publisher's policy and may be subject to US copyright law. Please refer to the publisher's site for terms of use.



Theoretical and experimental investigation of haze in transparent aerogels

LIN ZHAO,¹ ELISE STROBACH,¹ BIKRAM BHATIA,¹ SUNGWOY YANG,^{1,2}
ARNY LEROY,¹ LENAN ZHANG,¹ AND EVELYN N. WANG^{1,*}

¹Department of Mechanical Engineering, Massachusetts Institute of Technology, Cambridge, MA 02139, USA

²Currently with Chemical Engineering Department, University of Tennessee at Chattanooga, 615 McCallie Ave, Chattanooga, TN 37403, USA

*enwang@mit.edu

Abstract: Haze in optically transparent aerogels severely degrades the visual experience, which has prevented their adoption in windows despite their outstanding thermal insulation property. Previous studies have primarily relied on experiments to characterize haze in aerogels, however, a theoretical framework to systematically investigate haze in porous media is lacking. In this work, we present a radiative transfer model that can predict haze in aerogels based on their physical properties. The model is validated using optical characterization of custom-fabricated, highly-transparent monolithic silica aerogels. The fundamental relationships between the aerogel structure and haze highlighted in this study could lead to a better understanding of light-matter interaction in a wide range of transparent porous materials and assist in the development of low-haze silica aerogels for high-performance glazing units to reduce building energy consumption.

© 2019 Optical Society of America under the terms of the [OSA Open Access Publishing Agreement](#)

1. Introduction

Silica aerogels have been used for a variety of applications across many engineering and scientific disciplines, owing to their exceptional optical, thermal, and structural properties [1]. These useful properties stem from the aerogel's unique microstructure, which consists of a randomly cross-linked silica particle backbone supporting a highly porous (porosity: 80-99%) network [2]. In particular, monolithic silica aerogels can be made both optically transparent and thermally insulating by ensuring a small, uniform particle and pore size [3]. Such transparent silica aerogels have great potential in applications such as solar-thermal energy conversion systems [4–8] and advanced glazing units [9–13]. In these applications, a monolithic aerogel layer replaces the commonly used air or vacuum gap to minimize heat loss and maximize solar transmittance. While the porous structure diminishes heat transfer through the aerogel layer, the refractive index mismatch between the silica particles and air causes visible light to scatter as it passes through the aerogel layer. This visible-light scattering gives rise to silica aerogel's signature blue tint and reduces total solar transmittance, resulting in significant efficiency reduction in solar-thermal conversion systems. More importantly, light scattering also degrades the visual experience by deviating a fraction of the transmitted light from its original propagating direction, causing the transmission to become more diffuse. Due to the loss of directionality, the diffusely transmitted light makes objects appear haze (low contrast) when viewed through an aerogel layer. Therefore, understanding haze and developing strategies to reduce it in transparent aerogels are of great importance for its applications in both solar-thermal systems and advanced glazing units.

The light scattering process in an aerogel layer is depicted in Fig. 1. Collimated light is incident on the upper boundary of the aerogel layer ($z = 0$) in the normal direction ($\theta = 0$). As the incident light propagates, it interacts with silica particles in the aerogel and changes its

propagation direction due to multiple scattering. This scattering results in diffuse transmission or diffuse reflection of light which leaves the aerogel from the lower and upper boundary, respectively. On the other hand, light transmitted without interacting with the aerogel results in direct transmission. The formal definition of haze [14] is

$$\text{Haze} = \frac{T_{\text{diffuse}}}{T_{\text{total}}} = \frac{T_{\text{diffuse}}}{T_{\text{diffuse}} + T_{\text{direct}}} \quad (1)$$

where T_{diffuse} , T_{direct} , and T_{total} are the normal-diffuse, normal-direct, and normal-total transmittance, respectively. (“Normal” represents normal incidence. The total transmittance, also known as the hemispherical transmittance, is the sum of the direct and diffuse transmittance). State-of-the-art glazing units, such as evacuated double-pane windows, typically have a solar transmittance of 70-90% and haze lower than 3% [15]. Although an aerogel window can have similar transmittance, it is very challenging to achieve such low haze due to the light-matter interaction with the porous aerogel structure. Therefore, to develop next-generation transparent aerogels for high-performance solar-thermal systems and glazing units, it is necessary to improve our fundamental understanding of haze via a systematic modeling framework.

Several works have characterized haze in aerogels by experimentally measuring diffuse and total transmittance [3,9,10,16–21]. Due to the drastically different sample parameters such as density, thickness, particle size and type (granular or monolithic), the experimental haze values reported in the literature range from around 10% to nearly 100%. To be able to interpret the wide range of experimental results and guide material design to achieve desired optical properties, a theoretical model is highly useful. Moreover, global design optimization in most applications requires simultaneous consideration of the aerogel’s optical, thermal, and structural properties. Thus, an accurate model capable of correlating the optical, thermal and structural properties of aerogels could be beneficial. However, theoretical investigation of haze in transparent aerogels has not been reported primarily due to the complex transport within the aerogel microstructure. The multi-scale nature of the problem – varying six orders of magnitude from the particle size (~10 nm) to the sample dimension (~1 cm) – makes directly solving Maxwell’s equations a computationally formidable task. Effective medium approximation, e.g., the Maxwell-Garnett mixing rule, has been applied to obtain the effective optical constants of silica aerogels [22]. However, since it models the aerogel as a homogeneous medium, the effective medium approximation is not able to estimate the diffuse transmittance and haze accurately.

In this work, we have developed an optical model using the radiative transfer equation [23–25], which explicitly includes information about the aerogel microstructure via the extinction coefficient and the scattering phase function. We validated the model using experimental measurements on transparent silica aerogel samples fabricated in our lab. Comparison of model predictions with experimental results measured using a UV-Vis spectrophotometer showed good agreement across the entire visible spectrum. We then used the validated model to perform a parametric study of haze and found that the haze is most sensitive to the mean particle size. Smaller particle size not only reduces the haze at a given aerogel thickness but also weakens its dependence on thickness. In addition, we developed a complementary approach that prescribes the aerogel properties required to achieve desired haze/transmittance targets. We believe this work advances the fundamental understanding of haze in a wide range of transparent porous materials and could help guide material development to achieve optimal optical performance.

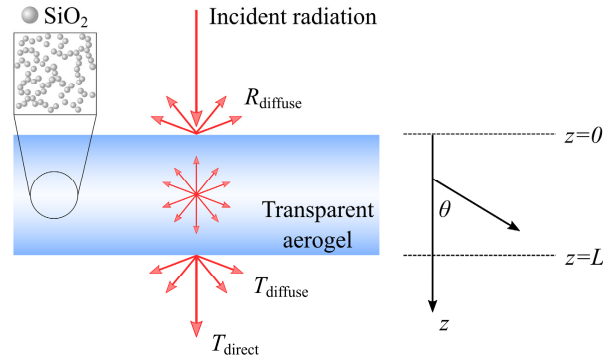


Fig. 1. Diffuse transmission caused by silica nanoparticle scattering in a transparent aerogel layer. In the typical plane-parallel geometry, the light intensity within the aerogel layer depends on the distance into the layer z and the polar angle θ as shown on the right.

2. Radiative transfer model

Light scattering by random media has been investigated for several applications. In particular, light management by scattering can enable efficient solar energy harvesting [26–32], efficient lighting [33], and zero-energy buildings [34]. Light scattering at random interfaces has also been extensively studied. Common analytical methods involve solving Maxwell's equations assuming a statistical distribution of the random interfaces [35,36]. However, the analytical methodology is difficult to generalize for 3D volumetric scatterers due to the large number of degrees of freedom [24,25]. To tackle this problem, we used the theory of radiative transfer, which is a powerful tool to describe radiative energy transfer in a random medium. Instead of solving for the electromagnetic field as in Maxwell's equations, the radiative transfer theory models the transport of specific intensity. The radiative transport theory has been successfully applied in the fields of astrophysics, atmospheric and oceanic science [23,37]. However, it has not been used to investigate haze and diffuse transmittance in aerogels [38,39].

In this work, we use the theory of radiative transfer to predict the haze and diffuse transmittance of transparent aerogels utilizing the knowledge of their basic physical properties. The first step is to establish a universal model for a generic random medium characterized by its material-dependent radiative parameters: optical depth, single scattering albedo, and scattering phase function. The next step is to link the aerogel microstructures to the radiative parameters in the model which can be accomplished by Mie theory. The light intensity within an aerogel layer is governed by the radiative transfer equation (RTE):

$$\mu \frac{dI_d(\tau, \mu)}{d\tau} = -I_d(\tau, \mu) + \frac{\omega}{2} \int_{-1}^1 P(\mu, \mu') I_d(\tau, \mu') d\mu' + \frac{\omega}{4\pi} P(\mu, \mu_0) F_0 e^{-\tau} \quad (2)$$

where $\mu = \cos(\theta)$ is the cosine of the polar angle θ , $\mu_0 = \cos(\theta_0) = 1$ represents the normal incident angle ($\theta_0 = 0$), $\tau = \beta z$ is the optical coordinate (β is the extinction coefficient, $\tau_0 = \beta L$ is the optical depth, L is the thickness of the medium), $I_d(\tau, \mu)$ is the diffuse intensity, ω is the single scattering albedo, $P(\mu, \mu')$ is the azimuthally averaged scattering phase function, and F_0 is the incident flux. By expressing the RTE in the form shown in Eq. (2), we assumed azimuthal independence and plane-parallel geometry as shown in Fig. 1. We also neglected the effect of polarization, as we are concerned only with un-polarized light (sunlight). The azimuthally averaged scattering phase function is defined as

$$P(\mu, \mu') = \frac{1}{2\pi} \int_0^{2\pi} d\phi \frac{1}{2\pi} \int_0^{2\pi} d\phi' P(\mu, \phi; \mu', \phi') \quad (3)$$

where $P(\mu, \phi; \mu', \phi')$ is the scattering phase function from angle (μ', ϕ') to angle (μ, ϕ) . To study the influence of different scattering mechanisms, three common phase functions were included in this work: isotropic, Rayleigh, and the Henyey-Greenstein (H-G) phase functions. The isotropic phase function, being the simplest, is a good approximation for scatterers smaller than the light wavelength. The Rayleigh phase function is the exact solution for small scatterers. The H-G phase function can describe scatterers larger than the light wavelength, which exhibit anisotropic scattering behaviors. The expressions for these phase functions are included in Eqs. (4)-(6),

$$P(\gamma) = 1 \quad (\text{Isotropic}) \quad (4)$$

$$P(\gamma) = \frac{3}{4}(1 + \cos^2(\gamma)) \quad (\text{Rayleigh}) \quad (5)$$

$$P(\gamma) = \frac{1 - g^2}{(1 + g^2 - 2g \cos(\gamma))^{\frac{3}{2}}} \quad (\text{Henyey - Greenstein}) \quad (6)$$

where γ is the angle between the scattering and incident directions, and g is a parameter to describe the scattering anisotropy. To solve Eq. (2), two sets of boundary conditions are necessary as shown in Eq. (7). The first boundary condition states that the incident diffuse intensity is zero in the positive z -direction. The second boundary condition requires no diffuse intensity at $z = L$ in the negative z -direction because of the low refractive index (~ 1) of aerogels (negligible reflection at $z = L$).

$$\begin{aligned} I_d(0, \mu) &= 0 \quad \text{for } 0 \leq \mu \leq 1 \\ I_d(\tau_0, \mu) &= 0 \quad \text{for } -1 \leq \mu \leq 0 \end{aligned} \quad (7)$$

With boundary conditions in Eq. (7) and phase functions in Eqs. (4)-(6), we numerically solved Eq. (2) by the discrete ordinate method (DOM) to obtain the diffuse intensity field [37]. The accuracy of our DOM solver was validated against published results and Monte Carlo ray tracing results on standard problems [23,40]. In all cases, the relative error was less than 0.1%. Once we obtained the diffuse intensity, we calculated the diffuse transmittance of a medium as shown in Eq. (8):

$$T_{\text{diffuse}} = \frac{2\pi \int_0^1 I_d(\tau_0, \mu) \mu d\mu}{F_0} \quad (8)$$

Figure 2(a) shows the result of diffuse transmittance as a function of the optical depth of a medium. We considered both pure scattering ($\omega = 1$) and partially absorbing ($\omega = 0.5$) media, as well as the influence of scattering anisotropy through the three phase functions described above. The diffuse transmittance in Fig. 2(a) shows an interesting behavior – it is nearly zero at small and large optical depths, but exhibits a maximum at an intermediate optical depth. This behavior is a result of weak scattering and low diffuse transmittance at small optical depths, and strong diffuse reflection which diminishes light transmittance at large optical depths. The maximum value of diffuse transmittance depends on both the scattering phase function and the scattering albedo. For the pure isotropic and Rayleigh scattering cases, the maximum diffuse transmittance is 0.35 at an optical depth of 2.05. For the pure forward dominant scattering case (H-G, $g = 0.5$), the maximum diffuse transmittance increases to 0.55 at an optical depth of 2.12. When the medium is partially absorbing, it lowers the diffuse transmittance and shifts the maximum diffuse transmittance point towards smaller optical depth as shown in Fig. 2(a).

Based on Beer-Lambert law, we know $T_{\text{direct}} = e^{-\tau_0}$ and $T_{\text{total}} = T_{\text{diffuse}} + T_{\text{direct}}$, which allows us to calculate haze using Eq. (1). Figure 2(b) shows the corresponding haze computed from the results in Fig. 2(a). The haze monotonically increases from zero to unity as the optical depth increases. A pure scattering medium has higher haze than a partially absorbing medium at the same optical depth since absorption does not contribute to haze and the contribution of scattering is reduced. The forward dominant H-G phase function also results in higher haze than the isotropic and Rayleigh scattering phase function due to the preferred forward directions leading to higher diffuse transmission.

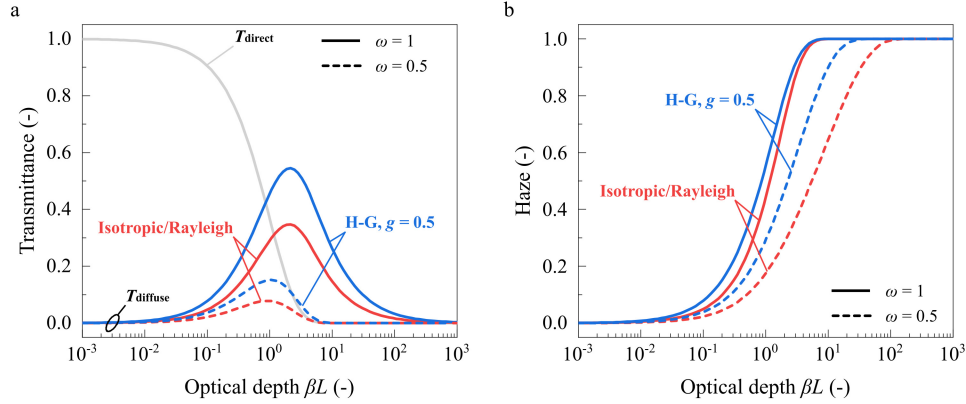


Fig. 2. a. Diffuse transmittance, b. Haze as a function of optical depth for isotropic, Rayleigh, and Henyey-Greenstein ($g = 0.5$) phase functions. The difference in diffuse transmittance and haze between isotropic and Rayleigh phase function is negligible. Results of both $\omega = 1$ (pure scattering medium) and $\omega = 0.5$ (partially absorbing medium) are shown.

3. Experimental validation

In this section, we compare and validate the predictions of the theoretical model with experimental measurements on transparent silica aerogel samples. We focus on the volumetric scattering effect and assume no scattering at the surface of the aerogel. This assumption should be reasonable for most cases since aerogel samples, fabricated in smooth molds, typically have optically flat surfaces. We used Mie theory to calculate the absorption (σ_{abs}) and scattering (σ_{sca}) coefficients as

$$\begin{aligned}\sigma_{\text{abs}} &= N\pi r^2 Q_{\text{abs}}(r, \lambda, n(\lambda)) \\ \sigma_{\text{sca}} &= N\pi r^2 Q_{\text{sca}}(r, \lambda, n(\lambda))\end{aligned}\quad (9)$$

where $N = 3\rho_{\text{ag}}/(\rho_{\text{silica}} 4\pi r^3)$ is the number density of silica particles in the aerogel (ρ_{ag} and ρ_{silica} are the aerogel apparent density and amorphous silica density respectively), r is the mean radius of the silica particles (modeled as spheres) within the aerogel, and Q_{abs} , Q_{sca} are the absorption and scattering efficiency calculated by Mie theory as a function of the particle size, wavelength, and the refractive index (n) of silica. The optical depth and single scattering albedo of the aerogel medium were calculated as $\tau_0 = (\sigma_{\text{abs}} + \sigma_{\text{sca}}) L_{\text{ag}}$ and $\omega = \sigma_{\text{sca}}/(\sigma_{\text{abs}} + \sigma_{\text{sca}})$ (where L_{ag} is the aerogel thickness). The scattering asymmetric factor g , obtained by Mie theory, was also incorporated in the H-G phase function to account for anisotropic scattering by large particles. By using Mie theory, we assumed independent, monodispersed, and spherical particles. For the case of transparent aerogels, this assumption works well because the particles only weakly scatter visible light and the particle filling factor is typically low (< 0.1). More sophisticated models that include dependent, polydispersed, and

non-spherical scatterers also exist which can be used to obtain the radiative parameters in such media [38,41,42].

To validate the model, we compared its predictions against experimental measurements on three aerogel samples with different densities and thicknesses (see aerogel synthesis in Appendix A and additional validation on high-haze commercial aerogels in Appendix B) [8,39]. The details of the three samples are summarized in Table 1. We performed optical measurements using a UV-Vis-NIR spectrophotometer (Cary 5000) equipped with an integrating sphere as shown in Fig. 3(a). Aluminum mirrors (Valumax Mirror, Newport) were mounted around the four side surfaces of the aerogel sample to minimize out scattering of light from the edges [43]. The total transmittance was measured by placing the sample at the inlet port of the integrating sphere and a diffuse reflector at the exit port. The diffuse transmittance was then measured by replacing the diffuse reflector with a light trap to remove the direct transmittance from the signal. All the measurements were conducted in the wavelength range from 220 nm to 1000 nm. An optical image of the aerogel (sample C), along with a piece of glass, is shown in Fig. 3(b) to illustrate the aerogel transparency.

Table 1. Transparent aerogel samples used in this study

Sample	Thickness (mm)	Density (kg/m ³)	Optical mean particle radius ^a (nm)	SAXS mean particle radius (nm)	Visible transmittance ^b (-)	Visible haze ^b (-)
A	4.75	144	3.05	2.99	0.981	0.0139
B	2.54	302	3.50	2.85	0.976	0.0284
C	5.26	293	3.50	2.88	0.937	0.0597

^aObtained by fitting the experimental total transmittance, ^bWeighted by the CIE Standard Illuminant C spectrum [14].

To use the developed radiative transfer model, we need to evaluate the mean radius r of the silica particles within the aerogel. We accomplished this by adjusting the only free parameter r in the model to achieve the best fit of the experimental total transmittance data for each sample as shown in Fig. 3(c) (top row). We compared the mean particle radius r from our optical fitting result to that from the Small Angle X-ray Scattering (SAXS) measurement, which is an established technique to measure the mean particle radius. As shown in Table 1, the optical and SAXS results are in good agreement. The small difference could be due to the different assumptions in the models used to extract the SAXS and optical mean particle radii and because the two measurements were not conducted on the same volumetric location of the sample.

Once we obtained the optical mean particle radius, we applied the model to predict the diffuse transmittance and haze of each sample. Figure 3(c) (middle and bottom row) compares the model predictions and experimental results. The radiative transfer model accurately predicts the diffuse transmittance and haze of the aerogel samples in the entire wavelength range. Moreover, in the measured wavelength range, sample C achieves the maximum diffuse transmittance at an optical depth corresponding to a wavelength of 252 nm, as predicted by the model. The measured maximum diffuse transmittance of the sample (maximum $T_{diffuse} = 0.36$) agrees well with the model prediction for isotropic scatterers (maximum $T_{diffuse} = 0.35$).

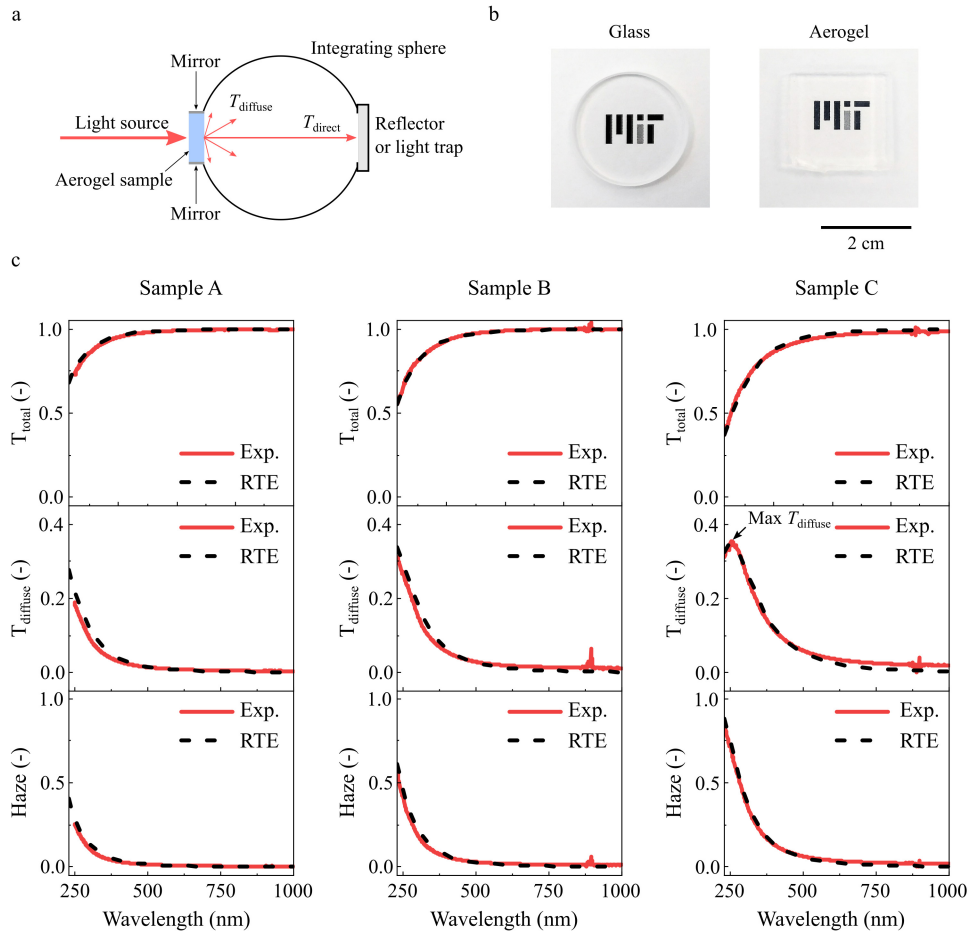


Fig. 3. a. Schematic of the diffuse and total transmittance measurement using a spectrophotometer with an integrating sphere. b. Optical image of a piece of glass and aerogel sample C (2 cm × 2 cm) on top of printed MIT logo. c. Measured and modeled total transmittance (top), diffuse transmittance (middle), and haze (bottom) of samples A, B, and C. The diffuse transmittance of samples A and B monotonically increases towards shorter wavelength, whereas the diffuse transmittance of sample C peaks at around 252 nm. This behavior confirms the model prediction as shown by the dashed lines.

4. Discussion

The validated theoretical model can be used to study the dependence of haze and total transmittance on aerogel physical properties to gain a better understanding and to guide design. We first studied the effect of mean particle size and aerogel density, which are intrinsic material properties. Figures 4(a) and 4(b) show the haze and total transmittance of a 5 mm thick aerogel layer as a function of its mean particle radius and density. The plots clearly show that the haze and total transmittance are very sensitive to the particle size. The haze increases from a few percent to more than fifty percent when the mean particle radius increases from 3 to 10 nm. From the contour plot, we can also obtain the required particle size to achieve a certain haze or total transmittance. As an example, to achieve a haze of less than 3%, the mean particle radius has to be smaller than about 5 nm for low-density aerogels ($\sim 50 \text{ kg/m}^3$). The requirement reduces to about 3 nm when the aerogel density approaches 300 kg/m^3 .

In addition to the particle size and density, the aerogel thickness is also an important parameter in many applications, especially when thermal performance is relevant. Figure 4(c) shows the haze and total transmittance as a function of the aerogel thickness for mean particle radii of 3, 6, and 9 nm. The aerogel density is fixed at 200 kg/m^3 . The results show a stronger thickness dependence of haze and total transmittance for larger particle sizes. When $r = 9 \text{ nm}$, the haze increases from 10% to more than 75% and the total transmittance decreases from 90% to less than 40% when the aerogel thickness varies from 1 mm to 20 mm. On the other hand, when $r = 3 \text{ nm}$, the increase in haze and decrease in total transmittance are comparatively small for the same aerogel thickness range. This result indicates that, for a given thickness range, a smaller particle size is preferable to achieve high-transparency, low-haze aerogels.

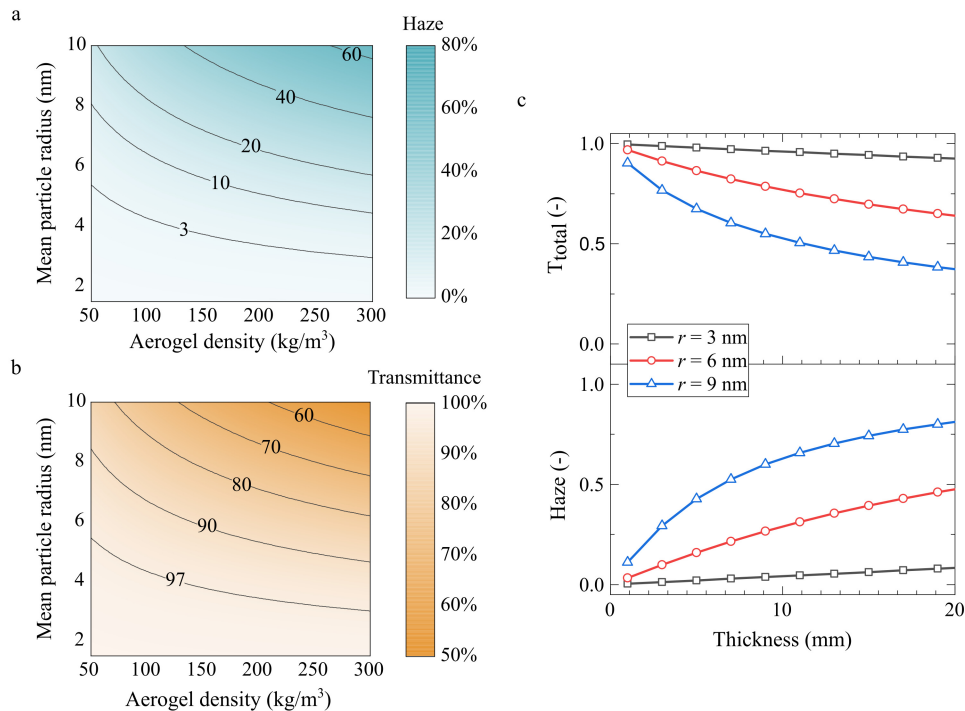


Fig. 4. a. Haze, b. Total transmittance of a 5 mm thick aerogel layer as a function of its mean particle radius and density; c. Haze and total transmittance as a function of aerogel thickness (aerogel density: 200 kg/m^3 , mean particle radius: 3, 6, and 9 nm).

To compare the aerogels developed in this work with silica aerogels reported in previous literature, we mapped each aerogel sample by its total transmittance (x-axis) and haze (y-axis) in Fig. 5. The total transmittance and haze were evaluated from the reported spectra and weighted by the CIE Standard Illuminant C spectrum. In this configuration, an ideal transparent aerogel resides in the bottom right corner (0% haze and 100% total transmittance). As shown in Fig. 5, previously reported aerogels are concentrated in the gray shaded area and are far from ideal. In comparison, the aerogel samples presented in this work have significantly better optical properties – haze about the same as single-pane glass and transmittance even greater than glass. Thus, these transparent aerogels could be promising spacer materials for high-performance glazing units.

In addition to experimental data, we also plotted the predicted relationship between total transmittance and haze by the theoretical model as solid lines in Fig. 5. Most experimental

data are clustered near the pure isotropic scattering case (gray line). Forward dominant scattering (red line) is likely to be the reason for data points slightly above the isotropic case because it results in higher haze at a given total transmittance. For data points below the isotropic case, absorption by impurities (blue line) lowers the total transmittance compared to the isotropic case. It is also worth noting from Fig. 5 that the total transmittance and haze are related. To achieve a haze value lower than a certain metric, there is a corresponding total transmittance metric that the aerogel needs to meet and vice versa. Considering the typical requirement of haze smaller than 3% [15] for a glazing unit, the requirement of total transmittance (70-90%) will be automatically satisfied if the haze target is met by the aerogel.

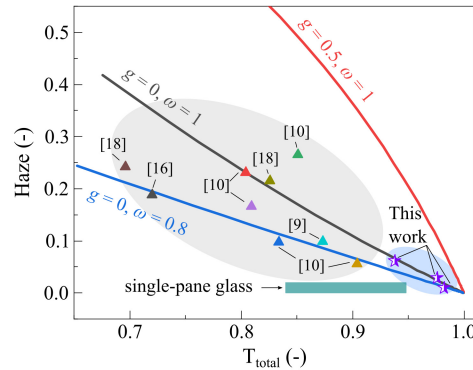


Fig. 5. Haze and total transmittance of transparent aerogels reported in previous literature (triangles) and demonstrated in this work (stars). Solid lines are the model predictions for different scattering asymmetric factor g and single scattering albedo ω . Performance of a single-pane glass is indicated by the green shaded area.

5. Conclusion

In summary, we developed an aerogel haze model based on the theory of radiative transfer. Mie theory was used to evaluate the radiative transport parameters based on the aerogel physical properties. We validated the model using experimental measurements on aerogel samples with different properties. Good agreement was achieved between the measurement results and model predictions. Using the validated model, we studied the dependence of haze on aerogel density, mean particle radius, and thickness. We also evaluated the combination of aerogel properties required to achieve certain haze/transmittance metrics. The fundamental insights gained from this study can help guide the design in many aerogel related applications. The general modeling framework developed in this work can also be extended to study a variety of transparent porous materials. Finally, the use of a high-transmittance and low-haze silica aerogel presented in this work as a spacer material in advanced glazing units and solar-thermal systems could help reduce our energy consumption significantly.

Appendix A: Aerogel sample fabrication

Two aerogel synthesis recipes were used to produce aerogel samples of different densities.

Recipe 1:

Sample A was synthesized by sol-gel polymerization of tetramethyl orthosilicate (TMOS, 131903, Sigma Aldrich), using an ammonia solution (NH_3 , 2.0M in Methanol, 341428, Sigma Aldrich) as a catalyst. TMOS was diluted by methanol (MeOH, 322415, Sigma Aldrich) followed by addition of NH_3 and water. The mixing molar ratio of chemicals was NH_3 :TMOS:water:methanol = 0.03:1:4.0:7.9.

Recipe 2:

Samples B and C were synthesized by replacing TMOS in recipe 1 with methyl silicate 51 (MS-51, CAS#12002-26-5, Austin Chemical Company) as the silicon precursor. The rest of

the recipe stayed the same. The mixing molar ratio of chemicals was $\text{NH}_3\text{:MS-51:water:methanol} = 0.001\text{:}1\text{:}12.4\text{:}18.6$.

After mixing the reactants, the solution was gelled in a disposable polystyrene container with optically flat internal surfaces. After aging for 3 days, the container was dissolved away using acetone. The mother solvent was replaced with ethanol (EtOH, 89234-848, VWR) to be prepared for critical point drying (CPD, model 931, Tousimis) as EtOH is miscible with liquid CO_2 . A bleed rate of 100 psi/hr was used to decrease the CPD chamber pressure from ~1300 psi to ambient pressure.

The dried aerogel samples were annealed at 400 °C for 12 hours to remove any residual organic species before optical measurements. For samples B and C, an additional annealing step at 600 °C for 6 hours was performed to further increase its density.

Appendix B: RTE model validation on high-haze aerogels

In addition to the low-haze aerogel samples, we also validated the RTE model on a high-haze sample. The sample was produced by Airglass (a Swedish aerogel company) and the optical data was reported by Buratti and Moretti [16]. The Airglass sample has a 19% haze (weighted by the CIE Standard Illuminant C spectrum). The measured and predicted haze are shown in Fig. 6. Good agreement is achieved between the experimental data and RTE model results.

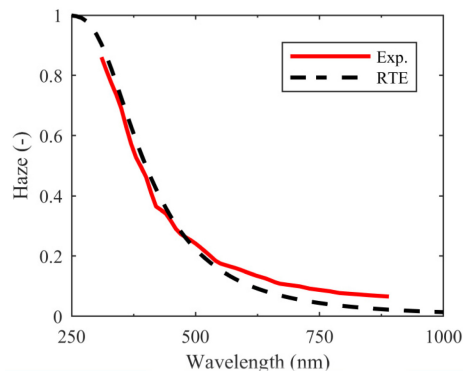


Fig. 6. RTE model validation on a high-haze aerogel sample (thickness = 14 mm, density = 150 kg/m³, optical mean particle radius = 10.1 nm).

Funding

ARPA-E FOCUS program (DE-AR0000471); Solid-State Solar Thermal Energy Conversion (S³TEC) Center, an Energy Frontier Research Center funded by the US Department of Energy, Office of Science, Basic Energy Sciences (DE-FG02-09ER46577); MIT Tata Center for Technology + Design

Acknowledgments

This work is supported as part of the ARPA-E FOCUS program under award number DE-AR0000471. This work made use of experiment facilities from the Solid-State Solar Thermal Energy Conversion (S³TEC) Center, an Energy Frontier Research Center funded by the US Department of Energy, Office of Science, Basic Energy Sciences under Award number DE-FG02-09ER46577. This work benefitted from SasView software, originally developed by the DANSE project under NSF award DMR-052054. L. Zhao acknowledges a graduate fellowship from the MIT Tata Center for Technology + Design. The authors would like to acknowledge Yoichiro Tsurimaki for valuable discussion and careful proofreading of the manuscript.

References

1. L. W. Hrubesh, "Aerogel applications," *J. Non-Cryst. Solids* **225**, 335–342 (1998).
2. M. A. Aegerter, N. Leventis, and M. M. Koebel, *Aerogels Handbook* (Springer, 2011).
3. G. M. Pajonk, "Transparent silica aerogels," *J. Non-Cryst. Solids* **225**, 307–314 (1998).
4. K. McEnaney, L. Weinstein, D. Kraemer, H. Ghasemi, and G. Chen, "Aerogel-based solar thermal receivers," *Nano Energy* **40**, 180–186 (2017).
5. S. Svendsen, "Solar collector with monolithic silica aerogel," *J. Non-Cryst. Solids* **145**, 240–243 (1992).
6. L. A. Weinstein, K. McEnaney, E. Strobach, S. Yang, B. Bhatia, L. Zhao, Y. Huang, J. Loomis, F. Cao, S. V. Boriskina, Z. Ren, E. N. Wang, and G. Chen, "A Hybrid Electric and Thermal Solar Receiver," *Joule* **2**(5), 962–975 (2018).
7. H. Kim, S. R. Rao, E. A. Kapustin, L. Zhao, S. Yang, O. M. Yaghi, and E. N. Wang, "Adsorption-based atmospheric water harvesting device for arid climates," *Nat. Commun.* **9**(1), 1191 (2018).
8. E. Strobach, B. Bhatia, S. Yang, L. Zhao, and E. N. Wang, "High Temperature Annealing for Structural Optimization of Silica Aerogels in Solar Thermal Applications," *J. Non-Cryst. Solids* **462**, 72–77 (2017).
9. M. Rubin and C. M. Lampert, "Transparent silica aerogels for window insulation," *Sol. Energy Mater.* **7**(4), 393–400 (1983).
10. K. Duer and S. Svendsen, "Monolithic silica aerogel in superinsulating glazings," *Sol. Energy* **63**(4), 259–267 (1998).
11. J. M. Schultz, K. I. Jensen, and F. H. Kristiansen, "Super insulating aerogel glazing," *Sol. Energy Mater. Sol. Cells* **89**(2-3), 275–285 (2005).
12. U. Berardi, "The development of a monolithic aerogel glazed window for an energy retrofitting project," *Appl. Energy* **154**, 603–615 (2015).
13. C. Buratti and E. Moretti, "Experimental performance evaluation of aerogel glazing systems," *Appl. Energy* **97**, 430–437 (2012).
14. "ASTM D1003-13 Standard test method for haze and luminous transmittance of transparent plastics," ASTM International, West Conshohocken, PA (2013).
15. ARPA-E SHIELD program, "Single-Pane Highly Insulating Efficient Lucid Designs," (U.S. DOE, 2015). <https://arpa-e.energy.gov/?q=arpa-e-programs/shield>.
16. C. Buratti and E. Moretti, "Glazing systems with silica aerogel for energy savings in buildings," *Appl. Energy* **98**, 396–403 (2012).
17. T. Gao, B. P. Jelle, T. Ihara, and A. Gustavsen, "Insulating glazing units with silica aerogel granules: The impact of particle size," *Appl. Energy* **128**, 27–34 (2014).
18. G. M. Pajonk, E. Elaloui, B. Chevalier, and R. Begag, "Optical transmission properties of silica aerogels prepared from polyethoxidisiloxanes," *J. Non-Cryst. Solids* **210**(2-3), 224–231 (1997).
19. A. Rigacci, F. Ehrburger-Dolle, E. Geissler, B. Chevalier, H. Sallée, P. Achard, O. Barbieri, S. Berthon, F. Bley, F. Livet, G. M. Pajonk, N. Pinto, and C. Rochas, "Investigation of the multi-scale structure of silica aerogels by SAXS," *J. Non-Cryst. Solids* **285**(1-3), 187–193 (2001).
20. C. Mandal, S. Donthula, R. Soni, M. Bertino, C. Sotiriou-Leventis, and N. Leventis, "Light scattering and haze in TMOS-co-APTES silica aerogels," *J. Sol-Gel Sci. Technol.* **2018**, 1–13 (2018).
21. Q. Liu, A. W. Frazier, X. Zhao, J. A. De La Cruz, A. J. Hess, R. Yang, and I. I. Smalyukh, "Flexible transparent aerogels as window retrofitting films and optical elements with tunable birefringence," *Nano Energy* **48**, 266–274 (2018).
22. J. S. Q. Zeng, R. Greif, P. Stevens, M. Ayers, and A. Hunt, "Effective optical constants n and κ and extinction coefficient of silica aerogel," *J. Mater. Res.* **11**(03), 687–693 (1996).
23. S. Chandrasekhar, *Radiative Transfer* (Dover Publications, 1960).
24. A. Ishimaru, *Wave Propagation and Scattering in Random Media* (Oxford University, 1997).
25. L. Tsang, J. Kong, and K. Ding, *Scattering of Electromagnetic Waves* (Wiley, 2000).
26. M. Zeman, O. Isabella, K. Jäger, R. Santbergen, S. Solntsev, M. Topic, and J. Krc, "Advanced light management approaches for thin-film silicon solar cells," *Energy Procedia* **15**, 189–199 (2012).
27. C. Lin and M. L. Povinelli, "Optimal design of aperiodic, vertical silicon nanowire structures for photovoltaics," *Opt. Express* **19**(Suppl 5), A1148–A1154 (2011).
28. C. Lin and M. L. Povinelli, "Optical absorption enhancement in silicon nanowire arrays with a large lattice constant for photovoltaic applications," *Opt. Express* **17**(22), 19371–19381 (2009).
29. F. Zhao, X. Zhou, Y. Shi, X. Qian, M. Alexander, X. Zhao, S. Mendez, R. Yang, L. Qu, and G. Yu, "Highly efficient solar vapour generation via hierarchically nanostructured gels," *Nat. Nanotechnol.* **13**(6), 489–495 (2018).
30. F. Jiang, H. Liu, Y. Li, Y. Kuang, X. Xu, C. Chen, H. Huang, C. Jia, X. Zhao, E. Hitz, Y. Zhou, R. Yang, L. Cui, and L. Hu, "Lightweight, Mesoporous, and Highly Absorptive All-Nanofiber Aerogel for Efficient Solar Steam Generation," *ACS Appl. Mater. Interfaces* **10**(1), 1104–1112 (2018).
31. H. Ghasemi, G. Ni, A. M. Marconnet, J. Loomis, S. Yerci, N. Miljkovic, and G. Chen, "Solar steam generation by heat localization," *Nat. Commun.* **5**(1), 4449 (2014).
32. G. Ni, N. Miljkovic, H. Ghasemi, X. Huang, S. V. Boriskina, C. Te Lin, J. Wang, Y. Xu, M. M. Rahman, T. J. Zhang, and G. Chen, "Volumetric solar heating of nanofluids for direct vapor generation," *Nano Energy* **17**, 290–301 (2015).

33. X. Liu, Y. Xiong, J. Shen, and S. Guo, "Fast fabrication of a novel transparent PMMA light scattering materials with high haze by doping with ordinary polymer," *Opt. Express* **23**(14), 17793–17804 (2015).
34. M. Zhu, J. Song, T. Li, A. Gong, Y. Wang, J. Dai, Y. Yao, W. Luo, D. Henderson, and L. Hu, "Highly Anisotropic, Highly Transparent Wood Composites," *Adv. Mater.* **28**(26), 5181–5187 (2016).
35. M. Sever, J. Krč, A. Čampa, and M. Topič, "Rigorous modelling of light scattering in solar cells based on finite element method and Huygens' expansion," *Opt. Express* **23**(24), A1549–A1563 (2015).
36. N. Sahraei, K. Forberich, S. Venkataraj, A. G. Aberle, and M. Peters, "Analytical solution for haze values of aluminium-induced texture (AIT) glass superstrates for a-Si:H solar cells," *Opt. Express* **22**(Suppl 1), A53–A67 (2014).
37. K. Stamnes, S.-C. Tsay, W. Wiscombe, and K. Jayaweera, "Numerically stable algorithm for discrete-ordinate-method radiative transfer in multiple scattering and emitting layered media," *Appl. Opt.* **27**(12), 2502–2509 (1988).
38. S. Lallich, F. Enguehard, and D. Baillis, "Experimental Determination and Modeling of the Radiative Properties of Silica Nanoporous Matrices," *J. Heat Transfer* **131**(8), 082701 (2009).
39. L. Zhao, S. Yang, B. Bhatia, E. Strobach, and E. N. Wang, "Modeling silica aerogel optical performance by determining its radiative properties," *AIP Adv.* **6**(2), 025123 (2016).
40. G. W. Kattawar, G. N. Plass, and S. J. Hitzfelder, "Multiple scattered radiation emerging from Rayleigh and continental haze layers. 1: Radiance, polarization, and neutral points," *Appl. Opt.* **15**(3), 632–647 (1976).
41. H. T. Yu, D. Liu, Y. Y. Duan, and X. D. Wang, "Theoretical model of radiative transfer in opacified aerogel based on realistic microstructures," *Int. J. Heat Mass Transf.* **70**, 478–485 (2014).
42. B. X. Wang and C. Y. Zhao, "Structural correlations and dependent scattering mechanism on the radiative properties of random media," *J. Quant. Spectrosc. Radiat. Transf.* **218**, 72–85 (2018).
43. A. Leroy, B. Bhatia, L. Zhao, and E. N. Wang, "Specular side reflectors for high efficiency thermal-to-optical energy conversion," *Opt. Express* **26**(10), A462–A479 (2018).